Scientific Reports

https://doi.org/10.1038/s41598-026-44456-x

Article in Press

Gas-bearing characteristics and its main controlling factors in low-rank coal seams of the Wujianfang Basin, North China

Received: 5 February 2026

Accepted: 11 March 2026

Published online: 13 March 2026

Cite this article as: Hu Y., Cai Y., Chen J. *et al.* Gas-bearing characteristics and its main controlling factors in low-rank coal seams of the Wujianfang Basin, North China. *Sci Rep* (2026). https://doi.org/10.1038/s41598-026-44456-x

Yingchun Hu, Yidong Cai, Jiamin Chen, Yunji Zhang, Kejian Zhao, Wei Chen & Meishan Gu

Gas-bearing characteristics and its main controlling factors in low-rank coal seams of the Wujianfang Basin, North China

Yingchun Hu[1,2], Yidong Cai[1,2,*], Jiamin Chen[1,2], Yunji Zhang[1,2], Kejian Zhao[1,2], Wei Chen[3], Meishan Gu[1,2]

[1]School of Energy Resources, China University of Geosciences, Beijing 100083, China

[2]Coal Reservoir Laboratory of National Engineering Research Center of CBM Development & Utilization, China University of Geosciences, Beijing 100083, China

[3]Tracy Energy Technologies, Beijing 100029, China

[*]email: yidong.cai@cugb.edu.cn

Abstract

The Erlian Basin stands as a potential region for low-rank coalbed methane (CBM) exploration and development in China. Located within the western part of this basin in Ujimqin Banner, the Wujianfang Basin hosts six exploitable coal seams and demonstrates significant potential for low-rank CBM production. However, the current understanding of the geological characteristics of CBM in this area remains limited, a challenge compounded by the substantial differences in reservoir attributes between low-rank and medium-to-high-rank CBM systems. This study utilizes a comprehensive dataset obtained from exploration activities since 2007, integrated with core observations and laboratory analyses, to investigate the coal quality, pore structure, isothermal adsorption, and gas-bearing characteristics of the coal seams in the Wujianfang Basin. Key findings reveal that the measured gas content in the parameter well varies between 0.453 m^3/t and 1.85 m^3/t, with methane constituting 48.18% to 83.21% of the total gas volume, which reflects a heterogeneous gas accumulation pattern across the basin. Gas content is strongly influenced by trapping and preservation conditions, with high-gas-content potential being governed by the combined effects of gas generation, migration, trapping, and preservation processes. Through the application of partial least squares regression (PLSR), volatile matter content, porosity, and fixed carbon content were identified as the main geological factors controlling gas enrichment in the basin. This research provides a theoretical foundation for advancing the study of gas-bearing properties in low-rank coals and

contributes to the basis for efficient CBM extraction under China’s dual-carbon strategy.

Keywords:

Wujianfang Basin, Low-rank coal, Gas-bearing, Main Controlling Factors, Partial Least Squares Regression (PLSR)

1. Introduction

Coal has been a cornerstone of the global energy supply for centuries, providing thermal energy, electricity, and raw materials for valuable industrial products[1]. Its complex pore structure hosts significant volumes of coalbed methane (CBM), which consists predominantly of methane[2-3]. In China, the estimated resources of low-rank CBM are approximately $14.7\times10^{12}m^3$, accounting for over 40% of the nation's total CBM resources[4]. In recent years, the CBM industry has increasingly shifted its research and development focus toward low-rank coal regions[5-6]. Enhanced national policy support has facilitated breakthroughs in gas production under specific conditions in provinces such as Shanxi, Xinjiang, Jilin, and Inner Mongolia. Nonetheless, exploration and development activities in most of these areas remain limited, and large-scale or commercial CBM production in China is still predominantly concentrated in medium- to high-rank coals[7].

Compared with medium- and high-rank coals, low-rank CBM reservoirs exhibit greater seam thickness, lower coalification, weaker methane adsorption capacity, lower gas content, and a significant proportion of biogenic gas[8]. Previous studies indicates that the enrichment and accumulation of low-rank CBM are primarily controlled by geological structure, burial depth, and hydrogeological conditions[9-13]. In the low-rank coals of the Junggar Basin, tectonic evolution controls the distribution of coal seams and the enrichment patterns of CBM, with different structural settings (such as shallow weak runoff zones and mid-deep stagnant flow zones) corresponding to distinct accumulation mechanisms[10]. Burial depth directly influences the coal seam gas content through geothermal temperature and pressure, with the gas content exhibiting an initial increase followed by a decrease as depth increases. There exists a critical depth: at depths shallower than this critical threshold, gas content rises with increasing pressure; beyond it, however, the elevated temperature leads to a decline in adsorption capacity, resulting in a reduction of gas content[11-12]. In the Xishanyao Formation of the southern Junggar Basin, the optimal burial depth for CBM accumulation ranges from 700 to 1000 meters[12]. Additionally, burial depth affects the physical properties of coal reservoirs: increased burial depth leads to reduced permeability, but ultra-deep layers (>1200 m) may form supersaturated gas accumulations[10]. Hydrogeological conditions determine the preservation and dissipation of CBM. In stagnant flow zones or runoff-stagnation transition zones, sluggish groundwater flow favors gas preservation, whereas in strong runoff zones, water flow tends to entrain and carry away the gas[10,13]. Methane genesis varies across different structural settings, exhibiting deep thermogenic gas, mid-depth secondary thermogenic gas trapped in structural culminations, and shallow biogenic gas accumulation [14-15].

Despite these insights, direct studies on how coal structure influences CBM adsorption-desorption behavior, gas-bearing characteristics, and well productivity in low-rank coals remain scarce both in China and internationally[7,16-18]. This work focuses on the low-rank coal seams of the Damoguaihe Formation in the

Wujianfang Basin. By integrating coal quality analysis, large-sample methane isothermal adsorption experiments, and CBM well parameter tests, it aims to reveal the geological and CBM characteristics of the low-rank coals. Using the partial least squares regression (PLSR) method, it quantitatively analyzes the controlling factors—such as coal quality, porosity, and geological conditions—on gas-bearing properties. The findings are expected to provide a reference for the development of low-rank CBM in the Erlian Basin and offer geological insights for coal mine gas control strategies.

2. Regional Geological Setting

The Erlian Basin, located in central and eastern Inner Mongolia Autonomous Region, has been identified as containing 47 coal-bearing basins with a total CBM-bearing area of 34,854 km^2 and geological CBM resources of $2.58\times10^{12}m^3$. It is regarded as a key strategic basin for achieving breakthroughs in the commercial development of China's low-rank CBM resources. The Erlian Basin, the largest Late Mesozoic fault-depression basin group in Inner Mongolia Autonomous Region, is composed of five depressions, one uplift, and over one hundred fault-depressed basins. It constitutes a significant coal-accumulating area from the Early Cretaceous coal-forming period in China[19]. The basin group is exceptionally rich in coal resources, with coalfields distributed from east to west, though most are developed in the eastern part, major coalfields include Shengli, Baiyinhua, Jilinguole, Baiyinhushuo, Bayanbaolige, Wennite, and Manite[20].

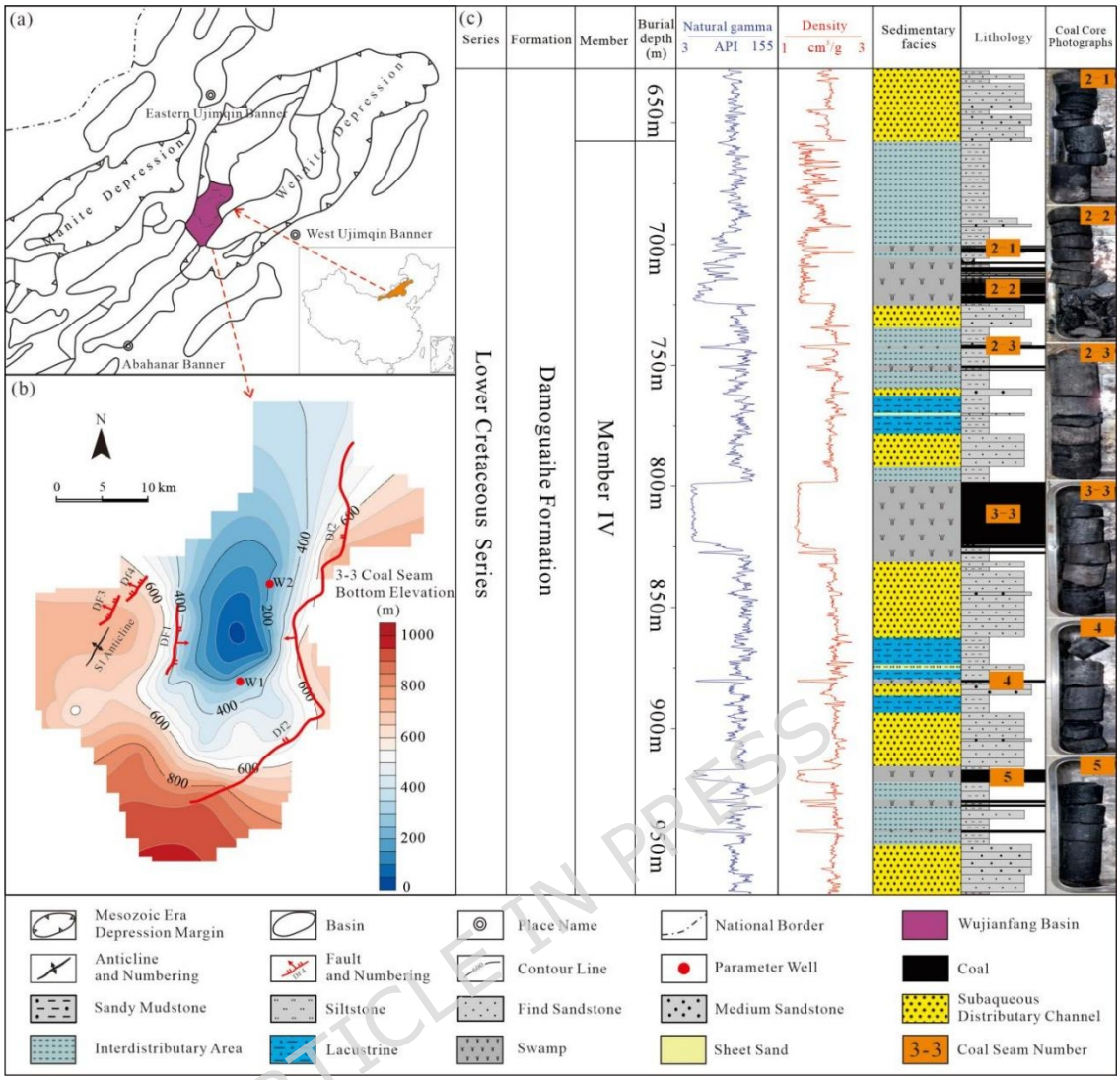

Fig 1. Location, Geological Overview, and Stratigraphic Columnar Diagram of the Wujianfang Basin: (**a**).Location of the Wujianfang Basin; (**b**). Geological Structure of the Wujianfang Basin; (**c**). Stratigraphic Column of the Damoguaihe Formation (W2 well).

The Wujianfang Basin, located in the Xiwuzhumuqin Banner, is part of the Early Cretaceous Erlian Basin structurally (Fig. 1a)[21]. It experienced two major orogenic events—the Yanshanian and Himalayan movements—which significantly reshaped the coal-bearing strata of the Damoguaihe Formation (Fig. 2)[22-27]. The basin exhibits a relatively simple internal structure, bounded by the syn-depositional master boundary fault F2 on its southeastern side and a smaller contemporaneous fault F1 on its southwestern side. The depositional center is located adjacent to the master boundary fault, while the basin floor morphology is narrow in the north and wide-gentle in the south, overall forming an irregular NE-trending half-graben fault-depression coal basin (Fig. 1b)[21,28]. The primary coal-bearing stratum in the basin is the Damoguaihe Formation (Fig. 1c), which contains six minable coal seams identified as 2-1, 2-2, 2-3, 3-3, 4, and 5. The coal ranks include lignite and

long-flame coal, both of which are classified as low-rank coals.

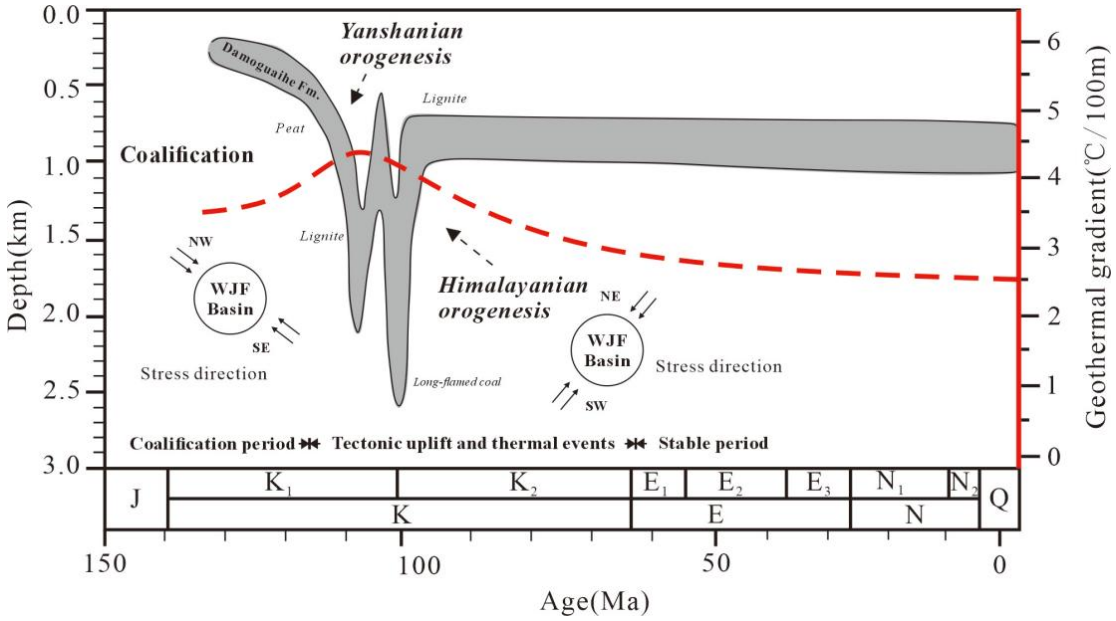

Fig 2. Generalized tectonic movement, temperature, and burial history curve for coal-bearing strata in the Wujianfang Basin.

3. Samples and Methods

3.1 Coal Samples and Basic Analysis

A total of 111 coal samples were primarily collected from different coal seams in the two parameter wells (W1 and W2) located in the northern and central parts of the basin. Prior to pore structure testing. Prior to pore structure testing, a series of standardized analyses were conducted on subsets of the coal samples: maximum vitrinite reflectance ($R_{o,max}$) was determined for 25 samples following Chinese National Standard GB/T 6948-2008；maceral composition was analyzed for 23 samples following Chinese National Standard GB/T 8899-2013；and proximate analysis was performed on 90 samples following Chinese National Standard GB/T 212-2008.

3.2 Low-temperature N2 adsorption experiment and High-pressure mercury intrusion (HPMI) experimen

Low-temperature N_2 adsorption experiments were primarily employed to characterize the volumes and specific surface areas of ultramicropores, micropores, and mesopores within the 1.7 nm~250 nm. The coal samples were analyzed using the low-temperature N_2 adsorption method in accordance with the Chinese National Standard SY/T 6154-2019. Mercury, being a non-wetting phase

for most core materials, can intrude into the pore space when the applied pressure equals or exceeds the capillary pressure of the pore throats, thereby overcoming the capillary resistance. By analyzing the volume of mercury intruded at progressively increasing pressures, intrusion-extrusion curves were generated for each sample, enabling the calculation of maximum mercury saturation and mercury withdrawal efficiency. The high-pressure mercury intrusion (HPMI) tests were conducted following the Chinese National Standard GB/T 21650.1-2008.

3.3 True Density, Apparent Density and Permeability Test

The porosity of the coal samples was calculated based on the true density and apparent density. The true density was determined in accordance with Chinese National Standard GB/T 217-2008, while the apparent density was measured following Chinese National Standard GB/T 6949-2010. Permeability tests were conducted according to Chinese National Standard GB/T 29172-2012.

3.4 Gas Content and Isotope Analysis

On-site desorption of coal samples was conducted using an constant-temperature water bath desorption setup to determine accurate gas content. Gas composition analysis was performed in accordance with the Chinese National Standard GB/T 13610-2020. Isotope testing was carried out at 25℃ employing a DELTA V ADVANTAGE mass spectrometer.

3.5 CH4 Isothermal Adsorption Experiment

Methane (CH_4) isothermal adsorption experiments were conducted in accordance with the Chinese National Standard GB/T 19560-2008. Each experiment comprised seven pressure points, with a maximum adsorption pressure of 12 MPa, and the temperature was set according to the actual formation temperature. This procedure was designed to determine the variation trend of the excess adsorption capacity of the coal samples under different pressure conditions.

3.6 Partial Least Squares Regression (PLSR)

Partial Least Squares Regression (PLSR) is a multivariate statistical data analysis method that integrates the advantages of multiple techniques, including multivariate linear regression, canonical correlation analysis, and principal component analysis. PLSR is particularly suitable for addressing challenges such as high-dimensional data with small sample sizes, avoiding overfitting, and scenarios where the number of predictors exceeds the number of observations.

The core idea of PLSR is to establish a linear regression model between the independent variables (X) and the dependent variables (Y) by projecting them into

a new latent variable space. The key advantage of PLSR is its effectiveness in handling scenarios where standard multiple linear regression struggles, particularly when dealing with small sample sizes, a large number of predictors, and severe multicollinearity. Under these challenging conditions, PLSR can still produce stable models with strong predictive capability.

The Variable Importance in Projection (VIP) was introduced to quantify the controlling influence of independent variables on the dependent variable(s). A VIP value greater than 1 indicates that the variable contributes significantly to the overall model performance and is considered an important predictor. Conversely, a VIP value less than 1 suggests a limited contribution, implying redundancy. Unlike conventional linear regression or grey relational analysis, PLSR accounts for interactive coupling among variables and can simultaneously handle multiple dependent variables (e.g. total gas content and methane content), making it a more comprehensive and systematic regression approach.

4. Results

4.1 Characteristics of Coal Seam Distribution

The coal seams of the Damoguaihe Formation in the Wujianfang Basin were primarily deposited within a delta-front–lacustrine sedimentary system, the main sedimentary microfacies identified include subaqueous distributary channels, interdistributary bays, swamps, and sheet sands (Fig. 3a). These facies provided multiple, recurrent favorable spaces for peat accumulation and coal seam formation. The coal seams generally occur at burial depths ranging from 600 to 1,000 meters (Fig. 3b). The 2 coal seam is predominantly developed in the northern part of the basin, with relatively thick accumulations observed in some wells. In contrast, the 4 and 5 coal seams are more developed in the southern part, though they are generally thinner overall. The 3-3 coal seam is the most continuous and stable seam, being widely distributed across most of the basin. In the central part of the basin, the 2 coal seam contains relatively well-developed gangue, including locally thick partings, while the other main coal seams have fewer and thinner gangue, with thick, single gangue occasionally observed in some wells.

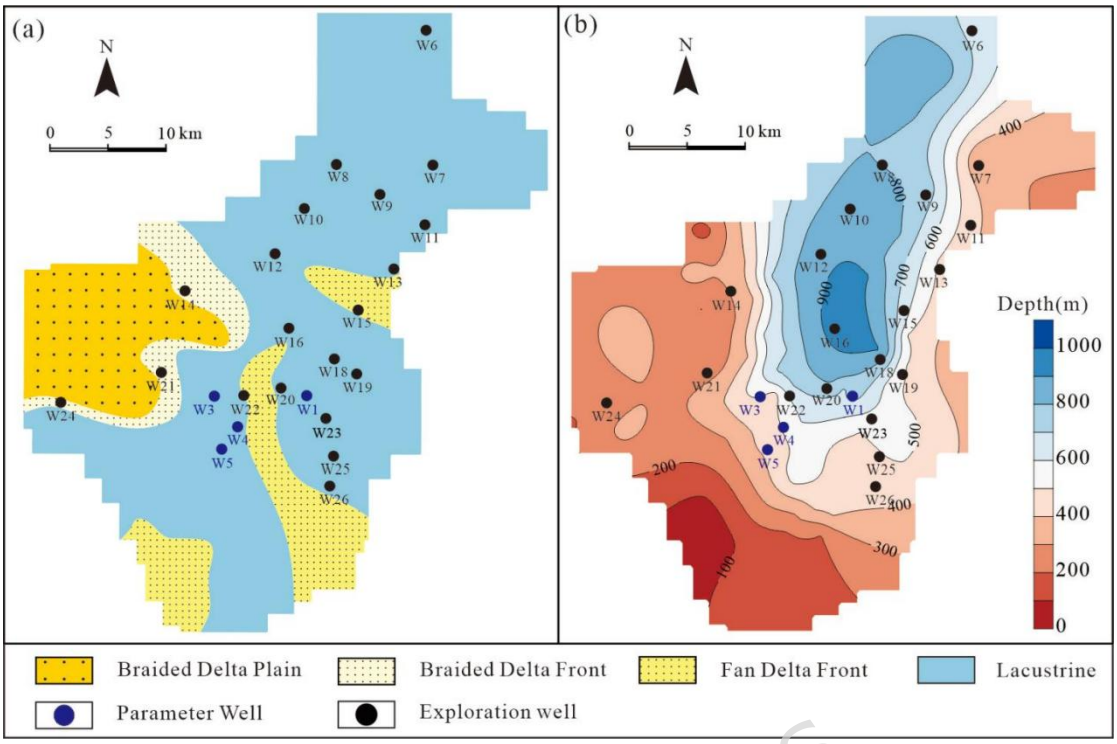

Fig 3. Depositional facies distribution and burial depth of the 3-3 coal seam in the Wujianfang Basin: (**a**). Distribution of 3-3 coal seam facies; (**b**). 3-3 coal seam burial depth.

4.2 Coal Quality Characteristics

Based on the on-site core observation results (Fig. 1c), the macroscopic lithotype boundaries of the coal samples from the Damoguaihe Formation are generally distinct, with identifiable maceral components. The macroscopically identified coal types in the basin are primarily lignite and long-flame coal., The macroscopic coal lithotypes are dominated by dull coal, followed by semi-dull coal. The maceral composition is predominantly durain with minor amounts of fusain, and the durain contains thin bands of bright coal. The $R_{o,max}$ of coal seams from the two parameter wells range between 0.37% and 0.57% (Table 1), with an average of 0.44%, indicating low-rank coals (lignite to sub-bituminous) and a relatively low maturity level.

The coal seams of the Damoguaihe Formation in the basin exhibit high organic matter content, with the maceral composition dominated by vitrinite, followed by inertinite, and a minimal presence of liptinite. Maceral analysis of coal samples from the W1 and W2 parameter wells (Table 1) reveals that the total organic maceral content ranges from 71.60% to 96.00%. Vitrinite is the predominant maceral, with contents ranging from 52.33% to 67.60% (avg. 59.45%), while inertinite content varies between 7.60% and 40.67% (avg. 26.91%). The total inorganic composition ranges from 4.00% to 28.40%, primarily consisting of clay minerals.

The proximate analysis of coal samples from the two parameter wells (Table 1)

yielded the following results: M_{ad} ranged from 5.05% to 8.69% (avg. 7.94%); A_{ad} varied between 6.58% and 35.40% (avg. 16.39%); V_{ad} content spanned 29.32%~38.22% (avg. 34.60%); and FC_{ad} fell within 26.91% ~49.96% (avg. 41.07). These data indicate that the coals from the Wujianfang Basin are characterized by low ash content, medium fixed carbon content, and relatively strong adsorption capacity. However, the presence of moisture and ash may partially attenuate their adsorption potential[29].

Table 1. Maximum vitrinite reflectance, proximate analysis, and maceral composition of of coal seam samples.

Coal seam	$R_{o,max}$ (min~max) avg	Macerals (%)				Proximate analysis (%)			
		V	I	E	M	M_{ad}	A_{ad}	V_{ad}	FC_{ad}
2-1	(0.40~0.43) 0.42	64.00	7.60	-	28.40	8.36	35.40	29.32	26.91
2-2	(0.43~0.45) 0.44	58.00	15.20	-	26.80	5.05	30.06	34.56	30.33
2-3	(0.42~0.42) 0.42	67.60	27.60	0.80	4.00	9.12	7.80	38.22	44.86
3-3	(0.37~0.45) 0.42	52.33	40.67	0.97	6.04	7.91	9.00	34.98	48.11
4	(0.44~0.57) 0.50	60.37	31.70	0.87	7.07	8.53	9.48	35.77	46.23
5	(0.43~0.50) 0.45	54.40	38.70	0.95	5.95	8.69	6.58	34.77	49.96

Note: V, I, E and M respectively represent the contents of Vitrinite, Inertinite, Exinite, and Minerals. Mad,Aad,Vad and FCad respectively represent the contents of moisture, ash, volatile matter and fixed carbon; '–' indicates that no data are available.

4.3 Pore Structure Characteristics

The low-temperature N_2 adsorption experiments were conducted to characterize the pore structure of the coal samples. The specific surface area was calculated using the BET (Brunauer-Emmett-Teller) multilayer adsorption model, while the pore volume parameters were analyzed based on the BJH (Barrett-Joyner-Halenda) theory and Kelvin equation to determine the distribution characteristics of micropores (<10 nm), small pores (10 nm~100 nm), mesopores (100 nm~1,000 nm), and macropores (>1,000 nm)[30-31]. The results (Table 2) indicate that the total pore volume ranges from 6.95×10^{-3} to 39.48×10^{-3} cm^3/g, with small pores (10 nm~100 nm) accounting for 40%~65% of the total volume, while meso- and macropores generally contribute less. The specific surface area varies between 3.63 m^2/g and 21.98 m^2/g, with micropores (<10 nm) contributing 67%~86% of

the total area, indicating that micropores are relatively well-developed compared to fine and mesopores in the coal samples.

Based on high-pressure mercury intrusion experiments conducted on five rock samples from different coal seams, the mercury intrusion curves and pore size increments are shown in Fig. 4. The coal seams of the Damoguaihe Formation in the Wujianfang Basin can be classified into two types: Type A (samples W2-1, W2-2 and W1-1), corresponding to 2-1,2-2 and 2-3 coal seams, exhibit relatively developed meso-macropores or microfractures, concentrated pore throats, and good connectivity of meso-macropores, which are favorable for the desorption of CBM; Type B (samples W2-3, W2-4, and W2-5), corresponding to 3-3, 4, and 5 coal seams, show developed fine, meso, and macro pores, with a higher proportion of fine throats and predominantly ink-bottle-shaped pores, resulting in overall poor pore connectivity .

Sample number	Coal seam	BET Specific surface area （m^2/g）	Total pore volume ($\times 10^{-3} cm^3/g$)	Average Pore size (nm)	Proportion of pore volume (%)			Proportion of Specific surface (%)		
					Microporous	Small pore	Mesopore	Microporous	Small pore	Mesopore
W2-1	2-1	21.98	39.48	7.24	57.90	40.60	1.60	86.20	13.80	0.10
W2-2	2-2	11.70	23.96	9.83	37.90	59.70	2.40	74.00	25.80	0.20
W2-3	3-3	3.63	6.95	13.94	26.80	64.40	8.80	67.00	32.20	0.80
W2-4	4	4.85	9.60	12.63	30.30	65.10	4.70	67.50	32.10	0.50
W2-5	5	7.48	11.19	11.19	31.70	63.30	5.00	73.90	25.70	0.40

Table 2. Pore volume and specific surface area results for liquid nitrogen experiments.

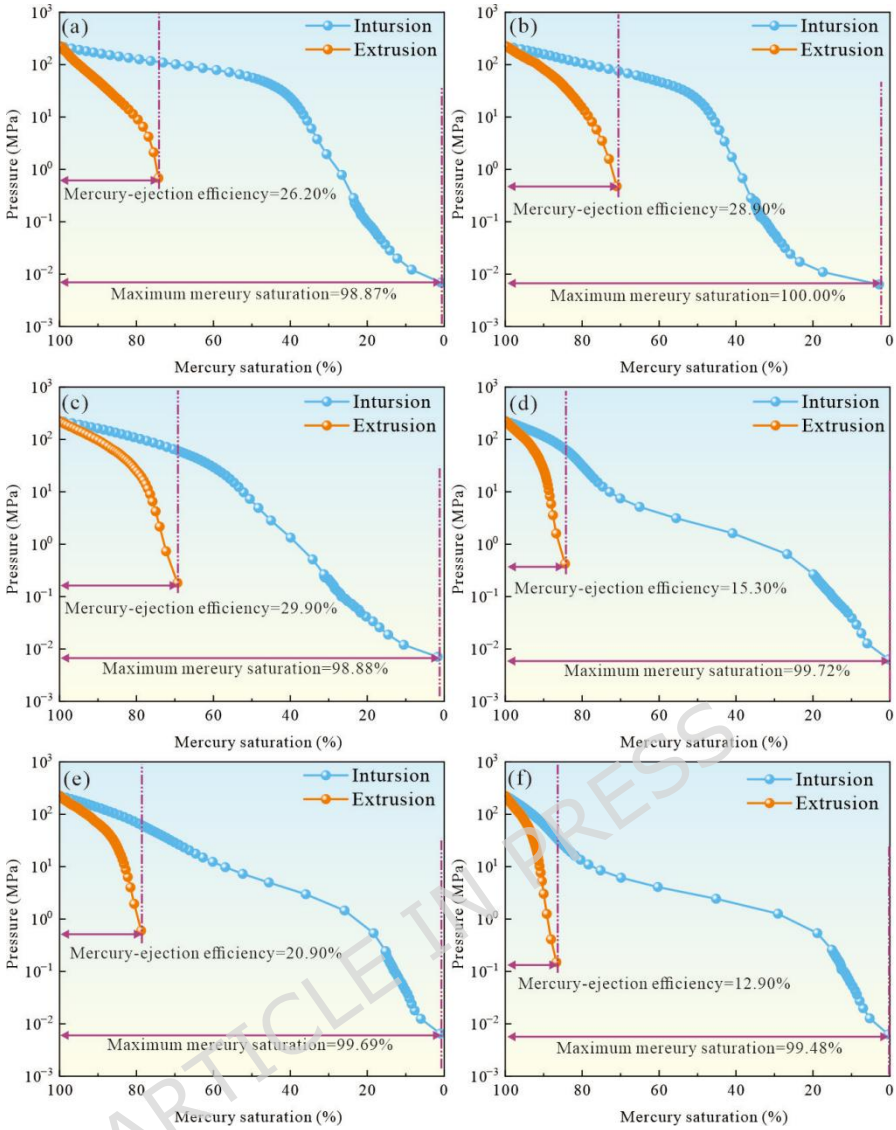

Fig 4. Coal mercury intrusion curves and pore size increment: (**a**). W2-1 Coal sample mercury intrusion curve; (**b**). W2-2 Coal sample mercury intrusion curve; (**c**). W1-1 Coal sample mercury intrusion curve; (**d**). W2-3 Coal sample mercury intrusion curve; (**e**). W2-4 Coal sample mercury intrusion curve; (**f**). W2-5 Coal sample mercury intrusion curve.

4.4 Characteristics of Porosity and Permeability Distribution

The porosity and permeability of coal samples from two parameter wells were tested. Porosity was calculated based on the true density and apparent density of the coal samples. The porosity analysis results (Fig. 5a) indicate that the porosity of each coal seam ranges from 8.15% to 10.67% (avg. 8.95%). Combined with the characteristic that the burial depth of the coal seams in the Damoguaihe Formation decreases from northeast to southwest, a negative correlation is observed between burial depth and porosity. This is primarily attributed to the gradual increase in geostatic stress with greater burial depth, which enhances

compaction effects as vertical stress rises[32].

The permeability of the coal seams in the Damoguaihe Formation ranges from 0.004 mD to 0.145 mD, with an average value of 0.060 mD (Fig. 5b). Relatively higher permeability values are observed in the 2-3 and 3-3 coal seams of the W1 well, reaching up to 0.154 mD and 0.130 mD, respectively. Similarly, the 3-3 coal seam in the W2 well also exhibits relatively high permeability. Combined with the characteristic that the burial depth of the Damoguaihe Formation coal seams decreases from northeast to southwest, the spatial variation in permeability shows a decreasing trend with increasing burial depth. Overall, the coal seams in the basin are classified as low-permeability reservoirs[33].

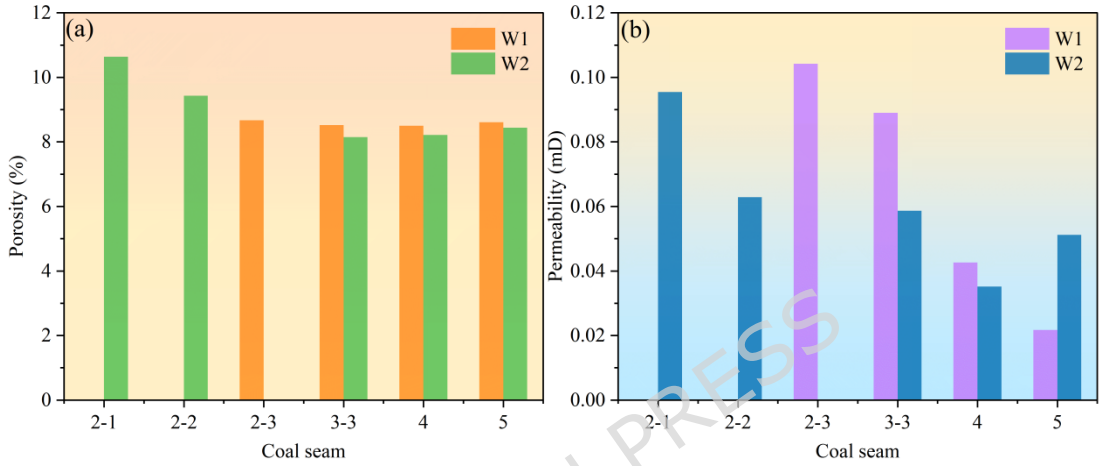

Fig 5. Results for coalbed porosity and permeability: (**a**). Results for coal seam porosity; (**b**). Results for coal seam permeability.

4.5 Sealing Characteristics of Roof and Floor

The analysis of roof and floor lithology and thickness for the six coal seams of the Damoguaihe Formation in the Wujianfang Basin, based on data from 82 exploration wells, reveals that the dominant roof and floor lithology is mudstone, with sandstone occurring in some areas. The roof thickness ranges from 0.15 m to 52.05 m, with mean values varying between 5.06 m and 6.72 m. The floor thickness ranges from 0.12 m to 57.74 m, with mean values varying between 4.92 m and 8.69 m. Four primary types of roof-floor lithological combinations were identified:sandstone-mudstone, mudstone-mudstone, mudstone-sandstone, and sandstone-sandstone. The mudstone-mudstone combination is the most developed, accounting for 55% of the occurrences across the study area, and is associated with the development of thicker coal seams.

The concept of a sealing coefficient is introduced to quantitatively analyze the impact of roof and floor lithology on the gas content of coal reservoirs, providing a direct reflection of the sealing capacity of the coal seam cover[34]. Based on the thickness and lithology of the coal seam roof and floor, an evaluation model for the sealing capacity of the coal seam roof and floor in the Wujianfang Basin is established (Formula 1):

$$C = \varepsilon * \tau \quad (1)$$

Where:C represents the sealing coefficient of the roof and floor. A higher value of C indicates a stronger sealing capacity of the cover layer. ε denotes the lithology evaluation factor of the roof and floor. τ represents the thickness of the roof and floor (in meters).

The compressive strength, tensile strength, and elastic modulus are commonly used to characterize the integrity of rocks. Higher values of these parameters indicate better roof and floor stability, stronger resistance to damage, and a lower propensity for fracture development[35-36].The lithology evaluation factor (ε) can be assigned based on the proportional product of these mechanical parameters (compressive strength, tensile strength, and elastic modulus) for different lithologies. In the Wujianfang Basin, the average compressive strength, tensile strength, and elastic modulus of mudstone are 17.52 MPa, 0.58 MPa, and 8.36 GPa, respectively. For sandstone, the average values are 14.34 MPa (compressive strength), 0.42 MPa (tensile strength), and 7.92 GPa (elastic modulus). Based on these mechanical parameters, the lithology evaluation factor (ε) is assigned as 0.64 for mudstone and 0.36 for sandstone in the model. The thickness (τ) of the coal seam roof and floor, which corresponds to the first overlying/underlying lithologic layer of the coal seam, is determined from the composite borehole histogram and well logging interpretation results.

The sealing coefficients of the coal seam roof and floor, calculated based on the evaluation model The roof sealing coefficient ranges from 2.24 to 3.45, with an average of 2.98, while the floor sealing coefficient ranges from 2.49 to 4.63, with an average of 3.16. The results indicate that for the 2-1 coal seam, the roof exhibits a stronger sealing capacity than the floor, contributing more significantly to gas containment. In the 2-2 coal seam, the roof's sealing performance is slightly better than that of the floor, with both demonstrating relatively good sealing properties in the northeastern part of the basin. For the 2-3 coal seam, the floor's sealing capability is marginally superior to the roof, and both show favorable sealing characteristics in the southern region. The 3-3 coal seam displays better sealing performance in the roof compared to the floor. In contrast, for the 4 coal seam, the floor's sealing capacity is significantly better than the roof, and this trend is even more pronounced in the 5 coal seam, where the floor's sealing ability is substantially stronger.

5. Discussion

5.1 Characteristics of Coalbed Gas Content

5.1.1 Characteristics of Gas Content

A systematic analysis of gas content and gas composition was conducted on coal samples from the W1 and W2 parameter wells, encompassing field desorption, lost

gas estimation, and residual gas measurement. The results of the gas content and composition analysis are summarized in Fig. 6. The gas content varies among different coal seams, with the average dry, ash-free total gas content ranging from 0.453 m^3/t to 1.85 m^3/t. Hydrocarbon gases in the seams are predominantly methane, accounting for 48.18% to 83.21% of the total gas volume. Nitrogen is the primary non-hydrocarbon gas, constituting 15.35% to 51.17% of the total gas, while carbon dioxide accounts for 0.87% to 4.94%. Additionally, trace amounts of ethane (0.19% to 0.22%) were detected in the 3-3, 4, and 5 coal seams of the W2 well. Among all seams, the 3-3 coal seam exhibits the highest gas content. Overall, the gas content of the six coal seams displays a unimodal distribution with depth.

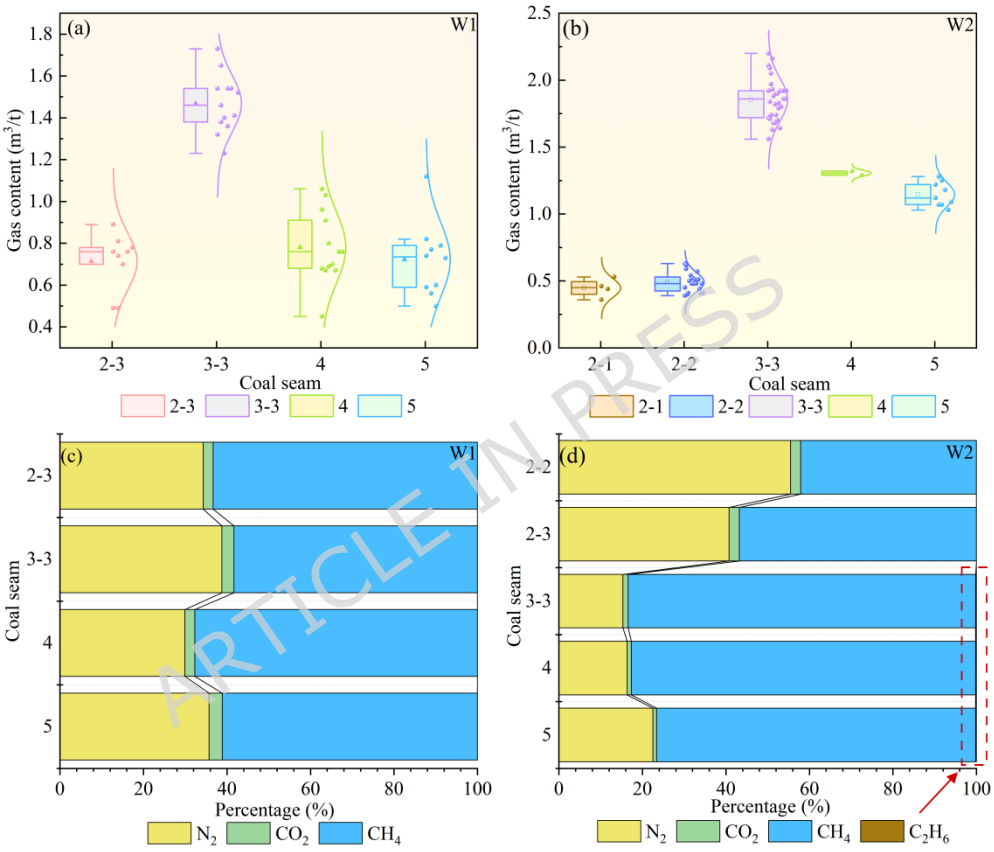

Fig 6. Results of coalbed gas content and composition: (**a**). Gas content for the W1 coal seam; (**b**). Gas content for the W2 coal seam; (**c**). Gas component for the coal seam in W1; (**d**). Gas component for the coal seam in W2.

The coal seams are thicker in the southern and eastern parts of the basin, as well as in local areas of the central-northern region, while they gradually thin towards the northern and southern margins. The western part generally exhibits smaller coal thicknesses (Fig. 7). The total coal thickness in the basin ranges from 0.45 m to 64.6 m, with an average thickness of 17.89 m. The recoverable coal content coefficient is 8.39%, indicating favorable coal-bearing properties. To further improve the accuracy of gas content inversion and better characterize the nonlinear relationship between gas content and multiple parameters, this study

introduces the XGBoost ensemble machine learning method. Based on seven parameters—gas content, depth, natural gamma ray, resistivity, coal thickness, and the thickness of mudstone in the roof and floor—from 117 sample data, gas content inversion was performed for the entire basin. On the training dataset, the XGBoost model achieved an R^2 of 0.91 and an RMSE of 0.166, demonstrating strong nonlinear fitting capability and stability. The trained model was then applied to the complete gas content dataset. In the dataset prediction, the XGBoost model performed most excellently, with an R^2 of 0.972 and an RMSE of 0.0918. Based on the XGBoost model inversion of gas content across all six coal seams in the entire basin, resulting in a predicted gas content distribution map (Fig. 7). The results reveal significant regional heterogeneity in the spatial distribution of gas content within the basin, which shows a strong correlation with the spatiotemporal migration characteristics of the coal accumulation centers.

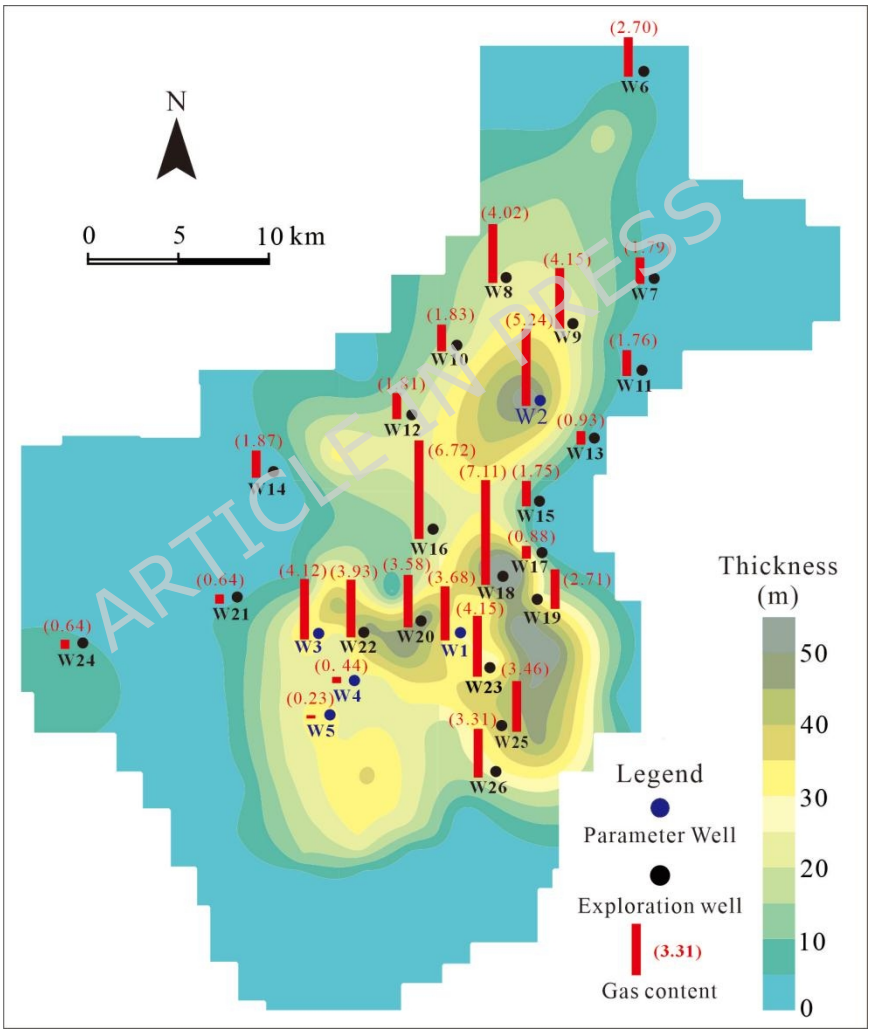

Fig 7. Total gas content and total coal seam thickness in the Wujianfang basin.

The early distribution of CBM content was characterized by high values in the central part of the basin and low values at the margins. As the depositional center and tectonic evolution adjusted, the center of coal seam development gradually

migrated from the central part of the basin toward the northeast, leading to a corresponding shift of high gas-content areas from the center to the northeastern region. Current predictive results indicate that the northeastern part of the study area is the primary zone for high CBM enrichment, while the northwestern part is dominated by low gas content or even undeveloped coal seams. The inverted gas content across the entire study area ranges from 0.08 to 1.85 m^3/t, reflecting a distinct differential accumulation pattern.

5.1.2 Adsorption Characteristics of CBM

The occurrence states of CBM in coal seams include adsorbed, free, and dissolved gas, with adsorbed gas being predominant. In low-rank coal CBM reservoirs, the gas primarily exists in both adsorbed and free states[4]. Low-rank coals are characterized by a high proportion of macropores and mesopores, a well-developed pore system, and consequently, a significant volume of free gas[37]. However, they exhibit a relatively weak adsorption capacity. Furthermore, due to their shallow burial depth (resulting in shorter migration pathways) and susceptibility to weathering effects, the CBM in these seams is prone to escape[10,38]. Investigating the adsorption performance of low-rank coals in the Wujianfang Basin through isothermal adsorption experiments will provide further insights into the gas-bearing characteristics and preservation conditions of the coal seams.

Based on the isothermal adsorption experiments conducted on coal samples from different coal seams of the W1 and W2 wells, the relationship between pressure and the dry, ash-free adsorption capacity is illustrated in Fig. 8a for the four coal seams of the W1 well and Fig. 8c for the five coal seams of the W2 well. The adsorption curves of the coal samples indicate that as pressure increases from 0 to 12 MPa, the adsorption capacity shows an increasing trend. The adsorption rate is relatively fast in the 0–5 MPa stage and then gradually slows down, eventually stabilizing. All curves conform to the characteristics of the Langmuir adsorption model[39-40]. The adsorption capacity of different coal seams varies significantly vertically, exhibiting strong heterogeneity[41-42].

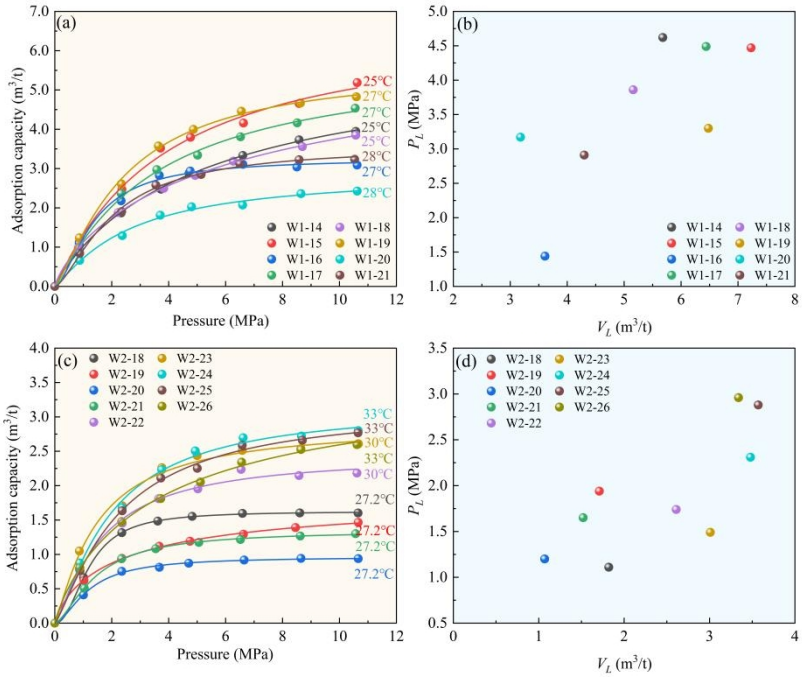

Fig 8. Isothermal adsorption results for coal samples from various coal seams: (**a**). W1well coal isothermal adsorption curve; (**b**). W1 well coal V_L-P_L relationship; (**c**). W2 well coal isothermal adsorption curve; (**d**). W2 well coal V_L-P_L relationship.

Note: W1-14 and W1-15 Samples, from 2-3 coal seam, tested at 25°C; W1-16 and W1-17 Samples, from 3-3 coal seam, tested at 27°C; W1-18 and W1-19 Samples, from 4 coal seam, tested at 27°C; W1-20 and W1-21 Samples, from 5 coal seam, tested at 28°C; W2-18 and W2-19 Samples, from 2-1 coal seam, tested at 27.2°C; W2-20 and W2-21 Samples, from 2-2 coal seam, tested at 27.2°C; W2-22 and W2-23 Sample, from 3-3 coal seam, tested at 30°C; W2-24 Sample, from 4 coal seam, tested at 33°C; W2-25 and W2-26 Samples, from 5 coal seam, tested at 33°C.

The Langmuir volume primarily reflects the adsorption capacity of coal. A higher value indicates stronger adsorption performance. The Langmuir pressure corresponds to the pressure at which the adsorption amount reaches half of the Langmuir volume. A higher Langmuir pressure suggests that CBM is more readily desorbed from the coal seam, which is favorable for CBM extraction. As shown in Fig. 8b and 8d, the Langmuir pressure for the W1 well ranges from 1.15 MPa to 4.62 MPa (avg. 3.44 MPa), while the Langmuir volume ranges from 1.93 m^3/t to 5.57 m^3/t (avg. 3.99 m^3/t). For the W2 well, the Langmuir pressure ranges from 1.11 MPa to 3.75 MPa (avg. 2.16 MPa), and the Langmuir volume ranges from 0.62 m^3/t to 4.04 m^3/t (avg. 2.29 m^3/t). The coal samples from the main coal seams in the W1 well exhibit a greater maximum adsorption capacity (higher Langmuir volume) and easier desorption during later production (higher Langmuir pressure). This may be related to their higher vitrinite content, as vitrinite typically provides

a larger specific surface area, offering more adsorption sites. In contrast, the lower Langmuir pressure of the W2 well coal samples suggests a relatively higher adsorption amount in the low-pressure range, indicating a stronger adsorption affinity for methane. This could also explain why the gas content of the main coal seams in the shallow sections of the W2 well is generally higher than that in the W1 well. Comprehensive analysis indicates that the Langmuir volume and Langmuir pressure within the basin exhibit a characteristic pattern of being higher in the south and lower in the north. This suggests that the coal in the W1 well has good adsorption capacity and significant potential for coal seam methane extraction.

5.1.3 Gas Genetic Types

The gas genetic types include thermogenic, biogenic, and mixed origins[43]. Biogenic gas can be further subdivided into primary biogenic gas and secondary biogenic gas. Low-rank CBM is predominantly of secondary biogenic origin, which is characterized by post-generation modification and serves as an important gas source supplement[44]. Classifying the gas genetic types primarily relies on the gas composition and chemical characteristics. CBM is generally considered to have two fundamental genetic types: biogenic and thermogenic. The methane carbon isotope value $\delta^{13}C(CH_4)$ of -55‰ is commonly used as the threshold for distinguishing between them: $\delta^{13}C(CH_4)\leq$-55‰ indicates biogenic gas, while $\delta^{13}C(CH_4)>$-55‰ suggests thermogenic gas[45-47]. Biogenic methane is generated mainly through two pathways: CO_2 reduction and acetate fermentation, these pathways can be distinguished based on the relationship between carbon and hydrogen isotopes ($\delta^{13}C(CH_4)$-$\delta D(CH_4)$)[48].

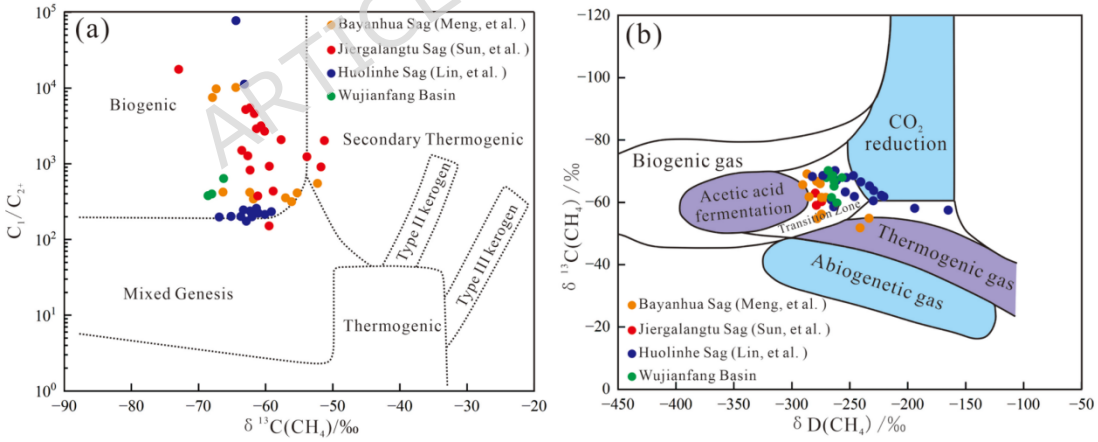

Fig 9. Petrogenetic combination identification map of CBM in the Wujianfang Basin: (**a**). C_1/C_{2+}-$\delta^{13}C(CH_4)$ Combined Identification Chart; (**b**). $\delta^{13}C(CH_4)$-$\delta D(CH_4)$ Combined Identification Chart.

The measured $\delta^{13}C(CH_4)$ values of CBM from drilled CBM wells in the Erlian Basin range from -69.4‰ to -61.1‰, and $\delta D(CH_4)$ values range from -272.7‰ to -230.6‰, indicating a transitional type between acetate fermentation and CO_2 reduction[43]. Isotopic analysis of coal samples from the Wujianfang Basin,

combined with a $\delta^{13}C(CH_4)$-C_1/C_{2+} identification diagram (Fig. 9a)[46,48-51], shows that $\delta^{13}C(CH_4)$ values are generally less than −60‰ and $\delta D(CH_4)$ values are less than −260‰, consistent with lacustrine biogenic gas characterized by high methane concentration and relatively simple gas composition. Furthermore, a ($\delta^{13}C(CH_4)$-$\delta D(CH_4)$) cross-plot (Fig. 9b) further indicates that the CBM in the Wujianfang Basin is predominantly generated via acetate fermentation, with a minor contribution from CO_2 reduction[46,48-51].

5.2 Factors Affecting Gas Content

The gas content within coal seams exhibits significant lateral variability across individual seams, vertical variability among different seams within a single well, and internal variability within thicker seams[52-54]. This heterogeneous distribution is governed by the coupled effects of various geological and hydrogeological factors, as well as reservoir heterogeneities[27,52,55-56].

Based on data from the W1 and W2 parameter wells, this study investigated the factors influencing the distribution of CBM content in the coal seams of the Damoguaihe Formation within the Wujianfang Basin, employing PLSR for quantitative analysis. The factors considered included coalification and coal characteristics, burial depth and thickness of the coal seams, sealing conditions, and structural controls. In addition to the parameters discussed in this study, other factors such as the tectonic setting, sedimentary conditions, and hydrogeological conditions also significantly influence the assessment of the gas-bearing property distribution in the basin's coal seams[57].

5.2.1 Coal quality, Ro,m and porosity

The gas content (both total gas content and methane concentration) within and between coal seams of the Wujianfang Basin exhibits notable variations, which can be explained by differences in coal quality and porosity. The properties of coal—including moisture, ash, volatile matter, and fixed carbon content—influence the maximum adsorption capacity primarily by altering pore characteristics. These factors are critical in controlling the total gas content and methane concentration in the coal seams [45;58].

The analysis of coal quality, $R_{o,m}$, and porosity parameters of the Wujianfang Basin effectively elucidates the variation patterns of total gas content and methane content with these factors. The results (Fig. 10a~d) indicate certain correlations between coal quality parameters (A_{ad}, V_{ad}, and FC_{ad}) and both total gas content and methane content. FC_{ad} shows a moderate positive correlation (R^2=0.40 and R^2=0.35), while A_{ad} (R^2=0.33 and R^2=0.25) and V_{ad} (R^2=0.35 and R^2=0.37) exhibit weak negative correlations. M_{ad} shows no significant correlation with total gas content or methane content. Differences in coal quality primarily influence gas content through variations in gas generation conditions and adsorption capacity. V_{ad} is an effective indicator of coalification degree[59-60]. These relationships demonstrate that ash and volatile matter contents influence the gas content of

various coal seams in the basin. As seen in Fig. 10e and 10f, no significant correlation is observed between total gas content/methane content and $R_{o,m}$, primarily because all sampled coal seams are low-rank coals with little variation in $R_{o,m}$ values. A moderate negative correlation (R^2=0.51) exists between gas content and porosity. This may be attributed to a large total pore volume but a small effective adsorption surface area, coupled with a high proportion of open pores that facilitate gas escape[61].

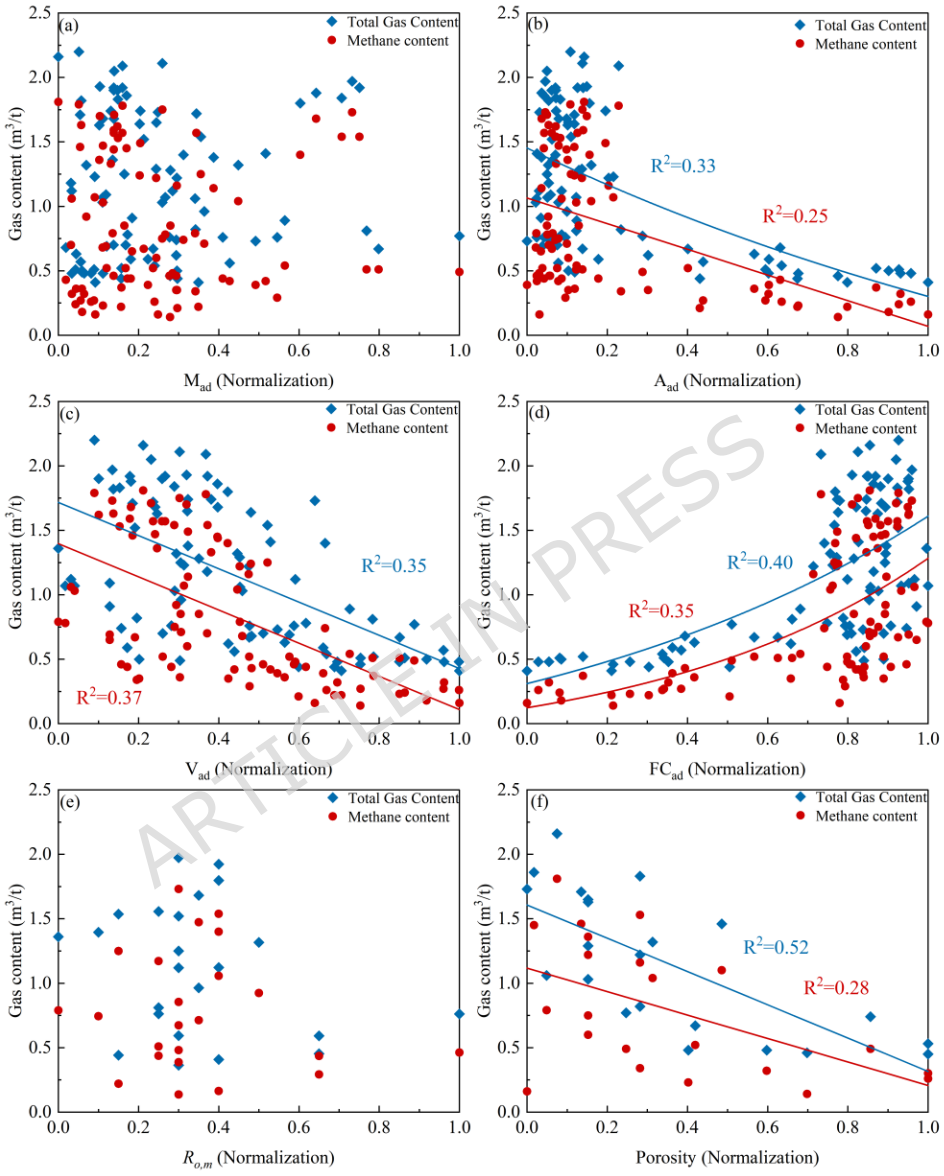

Fig 10. Relationship between coal quality, $R_{o,m}$, porosity, and total gas content,methane content: (**a**). Relationship between M_{ad} and total gas content,methane content; (**b**). Relationship between A_{ad} and total gas content,methane content; (**c**). Relationship between V_{ad} and total gas content,methane content; (**d**). Relationship between FC_{ad} and total gas content,methane content; (**e**). Relationship between $R_{o,m}$ and total gas content,methane content; (**f**). Relationship between Porosity and total gas content,methane content.

5.2.2 Burial depth and Thickness of coal seam

Previous studies have indicated that the burial depth of coal seams is one of the key factors controlling gas content[62-65]. The maximum burial depth governs coal formation and gas generation, while the present burial depth influences both gas content and preservation conditions[45,66-68].

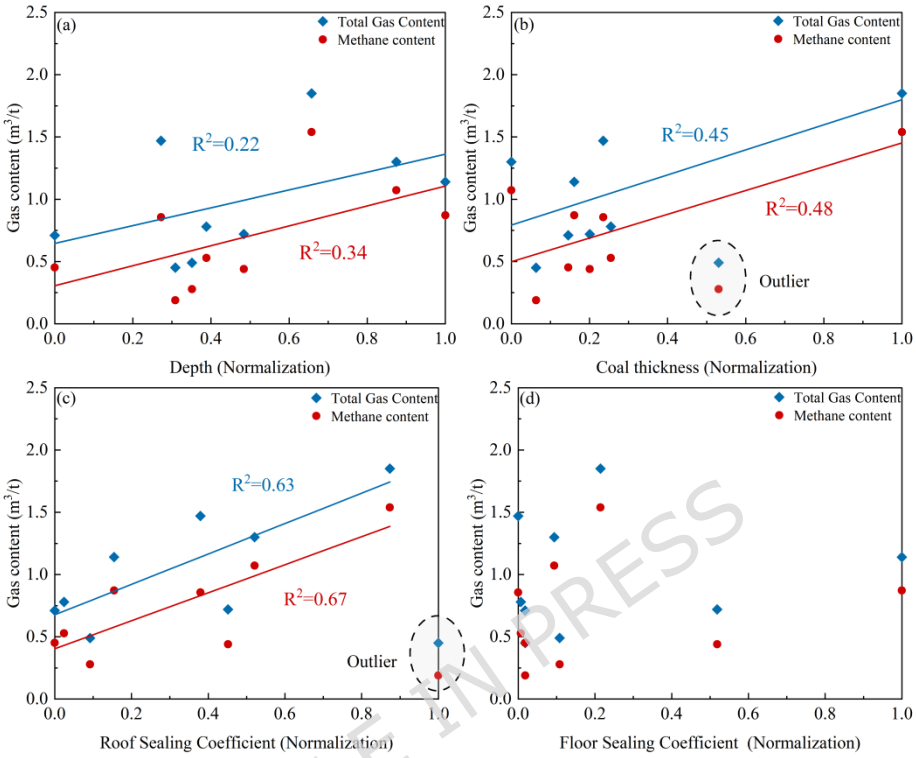

Fig 11. Relationship between Coal Seam depth, coal seam thickness, roof , floor Sealing Coefficient and total gas content,methane content: (**a**). Relationship between Coal Seam Depth and Total Gas Content, Methane Content; (**b**). Relationship between Coal Thickness and Total Gas Content, Methane Content; (**c**). Relationship between roof Sealing Coefficient and Total Gas Content, Methane Content; (**d**). Relationship between floor Sealing Coefficient and Total Gas Content, Methane Content.

The relationship between coal seam burial depth, thickness, total gas content, and methane content in the basin is illustrated in Fig. 11a and 11b. The total gas content shows a positive correlation with both burial depth and coal seam thickness (R^2=0.22 and R^2=0.45),. methane content exhibits a higher correlation with burial depth (R^2=0.34 and R^2=0.48). An outlier is observed in the burial depth and coal thickness corresponding to the 2-2 coal seam. This anomaly is likely associated with its depositional microenvironment during formation. The basin's coal seams were developed in a delta-front to lacustrine depositional system, and the 2-2 coal seam may have been closer to an underwater distributary channel or influenced by an interdistributary bay. This setting led to increased input of terrigenous clastics, resulting in a coal lithotype with higher ash content. The high ash content not only directly occupies adsorption sites and reduces adsorption

capacity but may also alter the pore structure-for example, by increasing the proportion of ineffective pores and degrading connectivity-through its influence on coal composition and diagenesis. Consequently, it diminishes gas-bearing potential jointly from the perspectives of both ‘storage space’ and ‘seepage pathways.’ These results indicate that burial depth and coal seam thickness jointly control the gas storage capacity of the coal seams.

5.2.3 Sealing capacity of the roof and floor

The relationship between the sealing coefficient of the roof and floor—calculated using the established evaluation model—and the total gas content and methane content is shown in Fig. 11c and 11d. The sealing coefficient of the coal seam roof shows a positive correlation with both total gas content and methane content (R^2=0.63 and R^2=0.67), while the sealing coefficient of the floor exhibits no significant correlation. An outlier is observed in the roof sealing coefficient corresponding to the 2-1 coal seam, which may be attributed to the relatively high ash content of the coal, resulting in inherently lower gas-bearing capacity. Given that the roof lithology is essentially consistent in the two parameter wells, it can be concluded that the roof plays a favorable role in natural gas preservation.

5.3 Analysis of Main Factors Affecting Gas Content

The study of controls on gas-bearing capacity has traditionally focused on univariate methods, primarily using simple linear regression to analyze the influence of individual variables on gas content, without conducting a comprehensive analysis of all variables collectively[69]. Many studies have employed grey relational analysis to identify the main controlling factors for gas-bearing capacity. However, this method assesses the degree of association based on the similarity in the geometric shapes of data sequences, which is inherently a linear approach and prone to misjudgment when dealing with nonlinear relationships[70]. In contrast, PLSR is used to establish regression models between multiple dependent and independent variables. It is particularly suitable for situations where multicollinearity exists among the multiple variables involved. In this study, using coal quality, porosity, coal seam burial depth, coal thickness, and the sealing coefficient of the roof and floor as independent variables, PLSR was performed to model their relationship with the total gas content and methane content of the coal seams.

The cumulative explained variance (R^2) for the dependent variable Y (total gas content/methane content) increased significantly from 73.1% with Factor 1 to 82.2% with Factor 2, a rise of 9.1 percentage points. This indicates that the second factor contributed substantial new and effective information. The adjusted R^2 reached its peak value of 0.763 at Factor 2. As this metric penalizes model complexity, a higher value suggests stronger predictive power and greater robustness. Starting from Factor 3, the adjusted R^2 began to decline consistently. This implies that the marginal gain in explanatory power from adding new factors (with R^2 only

increasing from 0.822 to 0.842) was insufficient to justify the increased model complexity. Instead, it introduced a higher risk of overfitting.

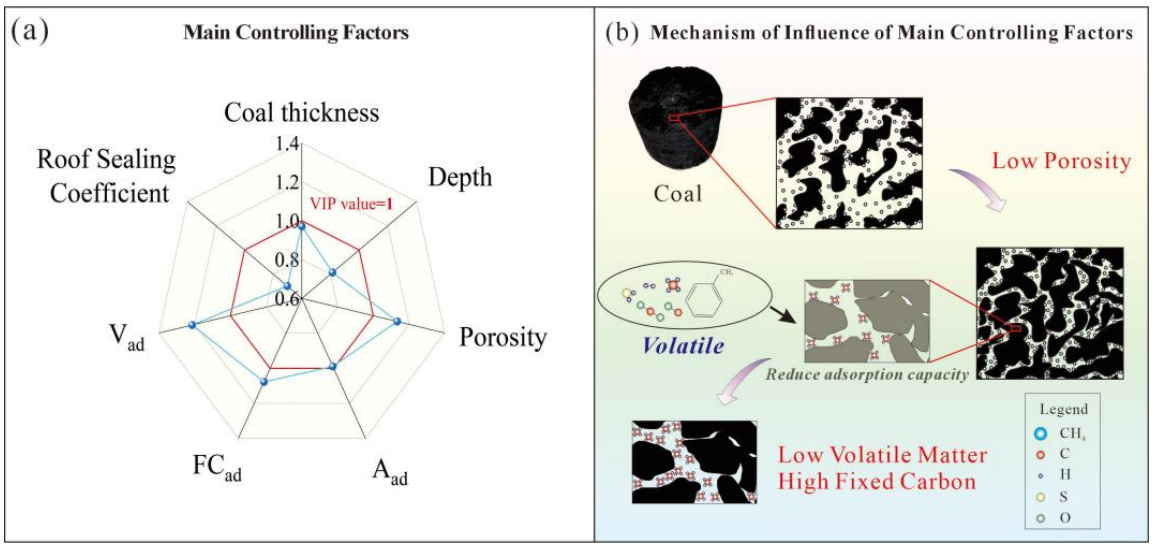

Fig 12. Mechanism of main controlling factors in the Wujianfang basin: (**a**). Main control factor radar chart; (**b**). Micro-level influence mechanisms of main control factors.

Based on the optimal number of factors (2 factors) determined, the Variable Importance in Projection (VIP) analysis of the seven independent variables revealed that V_{ad}, porosity, and FC_{ad} have VIP values greater than 1, indicating that these three parameters are the main controlling factors for the gas-bearing properties of the coal seams in the basin (Fig. 12a). A_{ad} content is identified as an important controlling factor (VIP value ≈1), while coal seam thickness, burial depth, and roof sealing coefficient are secondary controlling factors. These factors, under the geological background defined by the tectonic, sedimentary, and hydrogeological conditions of the basin, have organically coupled during their evolutionary processes to collectively control the gas-bearing characteristics of the coal seams.

The gas content of the coal seams in the Damoguaihe Formation is jointly controlled by the coupling of coal quality, burial depth, coal thickness, and roof sealing capacity. Volatile matter directly governs gas-bearing properties, porosity influences the reservoir space of the coal, and the weak negative correlation may be related to ineffective storage pores in low-rank coal. The adsorption sites provided by fixed carbon enhance gas content through positive contributions. Together, these three factors influence the 'generation-storage-adsorption' process of coal seam gas (Fig. 12b). The VIP value of ash content is close to 1, indicating it as an important controlling factor that directly affects the adsorption capacity and pore structure of the coal, thereby altering gas content. In contrast, the effects of coal thickness, burial depth, and roof sealing capacity are attenuated due to the dominant influence of these primary factors.

The gas-bearing characteristics of the coal seams in the Damoguaihe Formation of the Wujianfang Basin result from the multidimensional coupling of coal quality,

porosity, burial depth, and coal thickness under the specific geological setting of tectonic, sedimentary, and hydrogeological conditions. This multidimensional coupling mechanism collectively governs the development of methane-dominated gas occurrences and ultimately determines the gas potential of the coal seams.

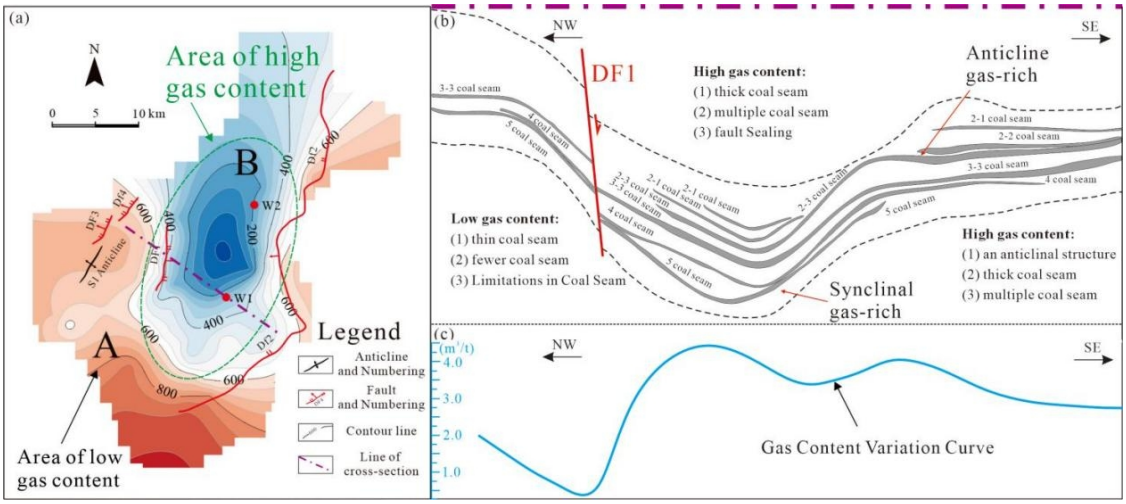

Fig 13. Evaluation subareas for CBM concentration potential in the Wujianfang basin: (**a**). Gas-bearing block delineation and profile orientation; (**b**). Coal seam profile; (**c**). Variation curve of gas content in the section.

Based on the trapping mechanisms and gas content, the CBM accumulation area can be divided into two blocks: the low-gas-content Block A and the high-gas-content Block B (Fig. 13). In Block A, the primary trapping mechanism is attributed to the favorable lithology of the roof strata, combined with moderate burial depth. However, the coal seams in this block are fewer in number, relatively thin, and limited in distribution. Consequently, these seams, along with the underlying strata, lack sufficient gas-generating capacity to accumulate adequate gas supply. In contrast, the formation of gas accumulations in Block B is primarily controlled by a suitable structural environment. Structural trapping plays a significant role in enhancing gas content here. In the central part of Block B, the accumulation of multiple, thick coal seams, coupled with fault sealing on the northwestern flank, makes this area a potential target for CBM development.

Based on the gas-bearing characteristics and its controlling factors and the delineation of blocks, combined with the coal quality, desorption characteristics, and seepage conditions of the six coal seams in the basin, a comprehensive analysis of the fracability and development potential of the reservoirs is conducted. Two main types of coal quality exist in the basin: coal with high vitrinite content and low mineral content, which is homogeneous in texture and conducive to the formation of longer main fractures; and coal with high inertinite or high mineral content, which exhibits heterogeneous mechanical properties and may promote the formation of complex fractures. Under the control of these coal quality backgrounds, the low permeability of type A coal seams suggests that they may possess a relatively more developed natural fracture system. Natural fractures serve as favorable weak planes for fracture initiation and propagation during

hydraulic fracturing, effectively reducing the breakdown pressure and contributing to the formation of a more complex fracture network, thereby enhancing the stimulated reservoir volume. In contrast, the overall poor pore connectivity of type B coal seams implies that their fracability may rely more on the ability to generate new main fractures. This comparison provides a geological basis for differentiated fracturing designs within the basin. By spatially coupling the analysis of ‘main controlling factors for gas-bearing,’ ‘desorption-seepage characteristics,’ and ‘geological conditions for fracability,’ this study not only deepens the theoretical understanding of reservoir gas content evaluation but also further advances the prediction from ‘resource-rich areas’ to 'producible sweet spots.' This offers more specific and reliable geological foundations for subsequent development well placement and fracturing process optimization.

This study also has several limitations that warrant clarification. First, the conclusions are primarily based on a limited dataset, including well logs and core samples from a small number of parameter wells. While these data provide crucial support, the restricted spatial coverage may not fully reflect the regional heterogeneity across the entire Wujianfang Basin, potentially affecting the analysis of coalbed gas content characteristics and controlling factors. Second, while the application of PLSR identified key controlling factors, it somewhat simplified the multi-factor coupled physical processes governing coalbed methane accumulation. Sedimentary, hydrogeological, and tectonic conditions within the basin were only briefly analyzed in this study. Future work should focus on expanding sampling and data acquisition networks to enhance spatial resolution, thereby providing deeper insights into the causal mechanisms of gas enrichment and predicting long-term recoverability.

6. Conclusions

This work reveals the gas properties together with its geological controls in the Damoguaihe Formation coal seams of the Wujianfang Basin with integrating coal quality analysis, large-sample methane isothermal adsorption experiments, and CBM well parameter tests. The primary conclusions are as follows:

(1) The coal seams of the Damoguaihe Formation in the Wujianfang Basin are generally buried at depths of 600-1000 m. The 3-3 coal seam is widely distributed across most of the basin, exhibiting relatively continuous and stable development. The total cumulative coal thickness in the basin ranges from 0.45 m to 64.6 m, with an average of 17.89 m. The recoverable coal-bearing coefficient is 8.39%, indicating favorable coal accumulation conditions.

(2) Pore characterization experiments on collected samples show that the six coal seams of the Damoguaihe Formation differ somewhat in pore structure, yet all display relatively high porosity and low permeability. A sealing evaluation model for the roof and floor of the coal seams was established, and the sealing capacity of each seam was systematically analyzed.

(3) Based on field gas-content measurements and basin-wide gas content

inversion, the spatial distribution of coal seam gas content generally exhibits a pattern of higher values in the central part of the basin and lower values at the margins. The adsorption capacity of the coal seams shows an increasing trend from north to south. Genetic analysis indicates that the CBM is of biogenic origin, primarily formed through acetic acid fermentation with accompanying CO_2 reduction.

(4) The gas-bearing characteristics of the coal seams are controlled by the coupled effects of coal quality, porosity, and geological conditions. PLSR analysis identifies volatile matter content, porosity, and fixed carbon content as the main controlling factors, which collectively govern the gas enrichment potential of the seams.This provides a more specific and reliable geological basis for subsequent well location selection and fracturing process optimization.

Data availability

The datasets generated and/or analyzed during the current study are not publicly available due to privacy considerations, but are available from the corresponding author upon reasonable request. Requests for data access will be reviewed by the research team to verify whether the request is subject to any intellectual property or confidentiality obligations.

References

1. Zhao, W., Cheng, Y., Pan, Z., Wang, K., & Liu, S. Gas diffusion in coal particles: A review of mathematical models and their applications. *Fuel*, **252**, 77-100. (2019)
2. Yan, F. et al. A novel ECBM extraction technology based on the integration of hydraulic slotting and hydraulic fracturing. *Journal of Natural Gas Science and Engineering*, **22**, 571-579. (2015)
3. Du, Z., Huang, Q., Guo, J., Gao, F., & Du, Y. The occurrence of nano-and micro-scale pores and their controls on the selective migration of gases in the coals of different ranks. *Fuel*, **264**, 116748. (2020).
4. Li, Y., Guo, T., Liu, X., & Peng, S. Resource potential and exploration targets of low-rank coalbed methane in China. *Oil & Gas Geology*, **45(6)**, 1537-1554. (2024).
5. Shao, L. et al. Selection of strategic replacement areas for CBM exploration and development in China. *Natural Gas Industry B*, **2(2-3)**, 211-221. (2015).
6. Zhang, Q. et al. Present situation and technical research progress of coalbed methane surface development in coal mining areas of China. *Coal Geology & Exploration*, **51(1)**, 2. (2023). (in Chinese with English abstract)
7. Xu, F. et al. The status and development strategy of coalbed methane industry in China. *Petroleum Exploration and Development*, **50(4)**, 765-783. (2023).
8. Li, L., et al.. Coalbed methane geology and exploration potential in large, thick,

low-rank seams in the Bayanhua Sag of the Erlian Basin, northern China. *Energy Exploration & Exploitation*, **40(3)**, 995-1022. (2022)

9. Fu, H. et al. Preliminary research on CBM enrichment models of low-rank coal and its geological controls: A case study in the middle of the southern Junggar Basin, NW China. *Marine and Petroleum Geology*, **83**, 97-110. (2017).
10. Li, X., Fu, X., Yang, X., Ge, Y., & Quan, F. Coalbed methane accumulation and dissipation patterns: a case study of the Junggar Basin, NW China. *Journal of Asian Earth Sciences*, **160**, 13-26. (2018).
11. Hou, H., Liang, G., Shao, L., Tang, Y., & Mu, G. Coalbed methane enrichment model of low-rank coals in multi-coals superimposed regions: a case study in the middle section of southern Junggar Basin. *Frontiers of Earth Science*, **15(2)**, 256-271. (2021).
12. Yuan, Y., Shan, Y., Tang, Y., & Cao, D. Coalbed methane enrichment regularity and major control factors in the Xishanyao Formation in the western part of the southern Junggar Basin. *Acta Geologica Sinica-English Edition*, **94(2)**, 485-500. (2020).
13. Du, Z., Zhang, X., Huang, Q., Zhang, S., & Wang, C. The gas content distribution of coal reservoir at the Changzhi block, south-central Qinshui Basin, North China: Influences of geologic structure and hydrogeology. *Energy Exploration & Exploitation,* **37(1)**, 144-165. (2019)
14. Lalk, E., Seewald, J., Bryndzia, L., & Ono, S. Kilometer-scale Δ13CH3D profiles distinguish end-member mixing from methane production in deep marine sediments. *Organic Geochemistry*, **181**, 104630. (2023)
15. Sano, Y. et al. Origin of methane-rich natural gas at the West Pacific convergent plate boundary. *Scientific Reports*, **7(1)**, 15646. (2017).
16. Wang, Z. et al. Changes in the anisotropic permeability of low-rank coal under varying effective stress in Fukang mining area, China. *Fuel*, **234**, 1481-1497. (2018).
17. Zhang, K., Jin, Y., Meng, Z., Wang, X., & Li, M. Experimental investigation on pore characteristics of heterogenous coal structures reservoir and coalbed methane diffusion/seepage behaviors. *Physics of Fluids*, **36(7)**. (2024).
18. Zheng, C., Chen, Y., Yu, L., Lei, W., Du, X., & Yang, F. Experimental investigation on pore characteristics of vitrain and durain in low rank coal based on fractal theory. *Scientific Reports*, **14(1)**, 5008. (2024).
19. Fu, S., et al. Tectono-stratigraphy characteristics of the Lower Cretaceous Saihantala Sag in the Erlian Basin, China: Normal faulting and controls on the depositional variability. *Journal of Petroleum Science and Engineering*, **195**, 107840. (2020).
20. Li, H., Qi, Q., Han, F., Zhang, P., Nie, Z., and Guan, X. Analysis of Low-rank Coal Distribution and Coalbed MethaneEnrichment Rules in Erlian Basin. *China Coalbed Methane*, **16(05)**, 19-23. (2019). (in Chinese with English abstract)
21. Fu, L., Zhuang, X., Li, J., and Pang, Q. The analysis on coal facies of coal seams in early CretaceousWujianfang coal basin, lnner Mongolia. *Coal Geology & Exploration*, **39(03)**, 1-6+13. (2011). (in Chinese with English abstract)

22. Tian, H. et al. Reservoir Characteristics and Diagenetic Evolution of Lower Cretaceous in Baibei Sag, Erlian Basin, Northern China. *Processes*, **13(5)**, 1391. (2025).
23. Wang, X. et al. Assessing the Depositional Environment of Cretaceous Ge-Rich Coals in the Wulantuga Mine, Shengli Coalfield, Northeastern China. Energy & Fuels, **38(4)**, 2777-2789. (2024).
24. Zuo, Y., Wang, C., Tang, S., & Hao, Q. Hao. Mesozoic and Cenozoic thermal history and source rock thermal evolution of the Baiyinchagan sag, Erlian Basin, Northern China, *Journal of Petroleum Science and Engineering*, **139**, 171-184. (2016).
25. Xu, W., Zhou, Y., Zhang, J., & Li, Y. Thermo-tectonic evolution of the northern Erlian Basin (NE China): Evidence from fission track and (U–Th)/He thermochronology. Journal of Asian Earth Sciences, **248**, 105620. (2023).
26. Wei, W., Zhu, X., Chen, D., Zhu, S., He, M., & Sun, S. Pore Fluid and Diagenetic Evolution of Carbonate Cements in Lacustrine Carbonate–siliciclastic Rocks: A Case from the Lower Cretaceous of the Erennaoer Sag, Erlian Basin, NE China. Journal of Sedimentary Research, **89(5)**, 459-477. (2019).
27. Cai, Y., Liu, D., Zhang, K., Elsworth, D., Yao, Y., & Tang, D. Preliminary evaluation of gas content of the No. 2 coal seam in the Yanchuannan area, southeast Ordos basin, China. *Journal of Petroleum Science and Engineering*, **122**, 675-689. (2014).
28. Liang, Y., Zhou, C., Lin, B. Survey Status and Analysis of the Wujianfang Coalfield. *Inner Mongolia Science Technology & Economy*, **(07)**, 21-24+26. (2009). (in Chinese)
29. Cheng, Y., Jiang, H., Zhang, X., Cui, J., Song, C., & Li, X. Effects of coal rank on physicochemical properties of coal and on methane adsorption. *International Journal of Coal Science & Technology*, **4(2)**, 129-146. (2017).
30. Brunauer, S., Emmett, P., & Teller, E. Adsorption of gases in multimolecular layers. *Journal of the American chemical society*, **60(2)**, 309-319. (1938).
31. Barrett, E., Joyner, L., & Halenda, P. The determination of pore volume and area distributions in porous substances. I. Computations from nitrogen isotherms. *Journal of the American Chemical society*, **73(1)**, 373-380. (1951).
32. Wang, Z., Xiong, J., Zhang, Y., Tao, G., Pan, J., & Niu, Q. Investigation of Permeability Stress Induced Damage Evolution of Shallow and Deep Coal Reservoirs in the Junggar Basin, China: Z. Wang et al. *Rock Mechanics and Rock Engineering*, 1-28. (2025).
33. Yi, X., Ding, Y., Wang, X., Lu, H., & Huang, G. The optimization of coal-bed methane completionand stimulation technologies. *Journal of China Coal Society*, **38(04)**, 629-632. (2013). (in Chinese with English abstract)
34. Xu, S. et al. Geological Controls on Gas Content of Deep Coal Reservoir in the Jiaxian Area, Ordos Basin, China. *Processes*, **12(6)**, 1269. (2024).
35. Shan, P., Li, W., Lai, X., Zhang, S., Chen, X., & Wu, X. Research on the response mechanism of coal rock mass under stress and pressure. *Materials*, **16(8)**, 3235. (2023).

36. Cai, Y., Zhou, X., Wang, L., Fu, Q., & Li, Q. Mechanical Damage Characteristics and Energy Evolution Laws of Primary Coal–Rock Combinations with Different Coal–Rock Ratios. *Applied Sciences*, **15(6)**, 3091. (2025).
37. Tao, S., Zhao, X., Tang, D., Deng, C., Meng, Q., & Cui, Y. A model for characterizing the continuous distribution of gas storing space in low-rank coals. *Fuel*, **233**, 552-557. (2018).
38. Lin, B., Li, H., Yuan, D., & Li, Z. Development and application of an efficient gas extraction model for low-rank high-gas coal beds. *International Journal of Coal Science & Technology*, **2(1)**, 76-83. (2015).
39. Xue, P., Zhang, L., Liang, Q., Sun, X., Zhao, Q., & Qi, P. Thermodynamic characteristics of CH4 adsorption by continental shale: A case study of the Upper Triassic Yanchang shale in the Yanchang Gasfield, Ordos Basin. *Natural Gas Industry B*, **7(3)**, 269-277. (2020).
40. Fianu, J., Gholinezhad, J., & Hassan, M. Application of temperature-dependent adsorption models in material balance calculations for unconventional gas reservoirs. *Heliyon*, **5(5)**. (2019).
41. Zhang, Z., Qin, Y., Yang, Z., Zhao, J., & Yi, T. Segmentation of multi-coal seam pore structure in single well profile and its sedimentary control: a case study of Well Y1 in Panguan syncline, western Guizhou, China. *Arabian Journal of Geosciences*, **12(15)**, 469. (2019).
42. Zhao, J., Xu, H., Tang, D., Mathews, J., Li, S., & Tao, S. Coal seam porosity and fracture heterogeneity of macrolithotypes in the Hancheng Block, eastern margin, Ordos Basin, China. *International Journal of Coal Geology*, **159**, 18-29. (2016).
43. Shen, J., Li, K., Zhong, H., Shabbiri, K., Hu, Q., & Zhang, C. The geochemical characteristics, origin, migration and accumulation modes of deep coal-measure gas in the west of Linxing block at the eastern margin of Ordos Basin. *Journal of Natural Gas Science and Engineering*, **91**, 103965. (2021).
44. Li, Y., Fu, H., Yan, D., Su, X., Wang, X., Zhao, W., Wang, H., & Wang, G. Effects of simulated surface freshwater environment on in situ microorganisms and their methanogenesis after tectonic uplift of a deep coal seam. *International Journal of Coal Geology*, **257**, 104014. (2022).
45. Scott, A. Hydrogeologic factors affecting gas content distribution in coal beds. *International Journal of coal geology*, **50(1-4)**, 363-387. (2002).
46. Van Voast, W. Geochemical signature of formation waters associated with coalbed methane. *AAPG bulletin*, **87(4)**, 667-676. (2003).
47. Li, Y., Tang, D., Fang, Y., Xu, H., & Meng, Y. Distribution of stable carbon isotope in coalbed methane from the east margin of Ordos Basin. *Science China Earth Sciences*, **57(8)**, 1741-1748. (2014).
48. Sun, Q. et al. Accumulation patterns of low-rank coalbed methane gas in theJiergalangtu Sag of the Erlian Basin. *Natural Gas Industry*, **38(04)**, 59-66. (2018). (in Chinese with English abstract)
49. Tao, J., Shen, J., Wang, J., Li, Y., & Li, C. Genetic Types and Exploration Prospect of Coalbed Methane inJiergalangtu Depression, Erlian Basin.

Geological Journal of China Universities, **25(02)**, 295-301. (2019). (in Chinese with English abstract)

50. Meng, Q., Li, L., Li, J., Tian, W., Lin, H., & Li, H. Genetic type and gas-generating potential of coalbed methane in theBayanhua Sag, Erlian Basin. *Coal Geology & Exploration*, **51(11)**, 24-33. (2023). (in Chinese with English abstract)
51. Lin H., Li L., Tang, S., Tian, W., Li, J., & Meng, Q. Origin and accumulation mechanisms of coalbed methane in low-rank coals in gas-rich sags in the Erlian Basin. *Coal Geology & Exploration*, **52(02)**, 60-69. (2024). (in Chinese with English abstract)
52. Scott, A., & Kaiser, W. Factors affecting gas-content distribution in coal beds: a review. *The AAPG/Datapages Combined Publications Database*, **July 28-31**, 101 - 106. (1996).
53. Bustin, R., & Clarkson, C. Geological controls on coalbed methane reservoir capacity and gas content. *International Journal of Coal Geology*, **38(1-2)**, 3-26. (1998).
54. Pashin, J. Variable gas saturation in coalbed methane reservoirs of the Black Warrior Basin: Implications for exploration and production. *International Journal of Coal Geology*, **82(3-4)**, 135-146. (2010).
55. Faiz, M., Saghafi, A., Sherwood, N., & Wang, I. The influence of petrological properties and burial history on coal seam methane reservoir characterisation, Sydney Basin, Australia. *International Journal of Coal Geology*, **70(1-3)**, 193-208. (2007).
56. Zou, Z., Liu, D., Cai, Y., Wang, Y., & Li, J. Geological factors and reservoir properties affecting the gas content of coal seams in the Gujiao Area, Northwest Qinshui Basin, China. *Energies*, **11(5)**, 1044. (2018).
57. Esen, O., Özer, S., Soylu, A., Rend, A., & Fişne, A. Geological controls on gas content distribution of coal seams in the Kınık coalfield, Soma Basin, Turkey. *International Journal of Coal Geology*, **231**, 103602. (2020).
58. Hu, Y., He, S., Qiu, F., Cai, Y., Wei, H., & Li, B. Full-Scale Pore Structure and Gas Adsorption Characteristics of the Medium-Rank Coals from Qinshui Basin, North China. *Processes*, **13(6)**, 1862. (2025).
59. Chandra, D., & Prasad, Y. Effect of coalification on spontaneous combustion of coals. *International Journal of Coal Geology*, **16(1-3)**, 225-229. (1990).
60. Laxminarayana, C., & Crosdale, P. Role of coal type and rank on methane sorption characteristics of Bowen Basin, Australia coals. *International Journal of Coal Geology*, **40(4)**, 309-325. (1999).
61. Yan, J., Meng, Z., Zhang, K., Yao, H., & Hao, H. Pore distribution characteristics of various rank coals matrix and their influences on gas adsorption. *Journal of Petroleum Science and Engineering*, **189**, 107041. (2020).
62. Drobniak, A., Mastalerz, M., Rupp, J., & Eaton, N. Evaluation of coalbed gas potential of the Seelyville Coal Member, Indiana, USA. International Journal of Coal Geology, **57(3-4)**, 265-282. (2004).

63. Li, Z., Liu, D., Ranjith, P., Cai, Y., & Wang, Y. Geological controls on variable gas concentrations: A case study of the northern Gujiao Block, northwestern Qinshui Basin, China. *Marine and Petroleum Geology*, **92**, 582-596. (2018).
64. Liu, H. et al. Block scale investigation on gas content of coalbed methane reservoirs in southern Qinshui basin with statistical model and visual map. *Journal of Petroleum Science and Engineering*, **114**, 1-14. (2014).
65. Scott, S., Anderson, B., Crosdale, P., Dingwall, J., & Leblang, G. Coal petrology and coal seam gas contents of the Walloon Subgroup—Surat Basin, Queensland, Australia. *International Journal of Coal Geology*, **70(1-3)**, 209-222. (2007).
66. Moore, T. Coalbed methane: A review. *International Journal of Coal Geology*, **101**, 36-81. (2012).
67. Ruppert, L., Hower, J., Ryder, R., Levine, J., Trippi, M., & Grady, W. Geologic controls on thermal maturity patterns in Pennsylvanian coal-bearing rocks in the Appalachian basin. *International Journal of Coal Geology*, **81(3)**, 169-181. (2010).
68. Su, X., Lin, X., Zhao, M., Song, Y., & Liu, S. The upper Paleozoic coalbed methane system in the Qinshui basin, China. *AAPG bulletin*, **89(1)**, 81-100. (2005).
69. Li, H. et al. Full-scale pore structure and its impact on methane adsorption in deep coal reservoirs of the Zijinshan area, Eastern Ordos Basin. *Physics of Fluids*, **37(8)**. (2025).
70. Zhang, J. et al. Coalbed Methane Productivity Prediction Using Gray Correlation Analysis and a GA-BP Neural Network: A Case Study in the Fukang Mining Area, Southern Junggar Basin. *ACS omega*, **10(47)**, 57692-57702. (2025).

Funding declaration

This research was funded by the National Natural Science Foundation of China (grant nos. 42372195 and 42130806), Scientific Research Innovation Capability Support Project for Young Faculty (grant no. ZYGXQNJSKYCXNLZCXM-E14) and the Fundamental Research Funds for the Central Universities (grant no. 2652023001).

Author contributions

Yingchun Hu: Writing – original draft, Investigation, Formal analysis. Yidong Cai: Writing – review & editing, Conceptualization, Methodology, Funding acquisition. Jiamin Chen: Methodology, Visualization. Yunji Zhang: Methodology, Technical assistance. Kejian Zhao: Methodology, Technical assistance. Wei Chen:

Methodology, Data support. Meishan Gu: Methodology, Technical assistance.

Declaration of competing interest

The authors declare that they have no known competing financial interests or personal relationships that could have appeared to influence the work reported in this paper.

Additional information

Correspondence and requests for materials should be addressed to Y.C.